Glass Package for Radar MMICs Above 150 GHz

THOMAS GALLER [1] (Graduate Student Member, IEEE), **TOBIAS CHALOUN** [1] (Member, IEEE),
WINFRIED MAYER [2] (Senior Member, IEEE), **KEVIN KRÖHNERT** [3], **DZMITRY STARUKHIN** [4],
NORBERT AMBROSIUS [5], **MALTE SCHULZ-RUHTENBERG** [5],
AND CHRISTIAN WALDSCHMIDT [1] (Senior Member, IEEE)

(Regular Paper)

[1] Institute of Microwave Engineering, Ulm University, 89081 Ulm, Germany
[2] Endress+Hauser SE+Co. KG, 79689 Maulburg, Germany
[3] Fraunhofer IZM, 13355 Berlin, Germany
[4] Sentronics Metrology GmbH, 68167 Mannheim, Germany
[5] LPKF Laser & Electronics AG, 30827 Garbsen, Germany

CORRESPONDING AUTHOR: Thomas Galler (e-mail: thomas.galler@uni-ulm.de).

ABSTRACT This work presents a novel sensor packaging and a novel transition concept for radar applications above 150 GHz based on glass material. By using laser induced deep etching (LIDE) technology, glass vias and cavities are fabricated without degrading the mechanical stability of glass, as micro-cracks are completely avoided. Especially at high millimeter wave (mm-wave) frequencies, precise structuring on low dielectric loss materials and a high integration density are essential for low loss transitions. In this paper, an ultra compact FMCW radar monolithic microwave integrated circuit (MMIC) at 160 GHz is used to demonstrate this packaging technology. In addition, the high frequency signal is guided by a low loss transition to a deposed antenna via a dielectric waveguide (DWG) providing the antenna front end with mechanical flexibility. Thus, using plated through glass vias (TGVs) and a circulating solder ring, the package is hermetically sealed. The optical transparent glass package has a size of only 5.8 mm × 4.4 mm × 0.9 mm. A minimum measured insertion loss of 2.85 dB at 162 GHz from chip to DWG is achieved. The complete radar system with a range resolution of 12 mm is demonstrated via radar measurement.

INDEX TERMS Glass, hermetically sealed, millimeter wave, MMIC, package, TGV, transition, interposer.

I. INTRODUCTION

The increased demand for low-cost and compact radar sensors in the last decades pushed the radar development to millimeter wave (mm-wave) frequencies. Driven by the automotive sector [1], many other industrial applications use small radars to sense their surrounding. High integration density on MMICs reduces the number of components on printed-circuit-boards (PCB) and thus the sensor price. Packaging these chips with RF signals above 150 GHz is challenging, as decreases in radiation efficiencies are provoked by Teflon based substrate materials and insufficient structuring accuracy.

Conventional solutions like quad-flat-no-lead (QFN) [2], [3] suffer from high dielectric losses due to epoxy based mold compounds. Hence, the radiation efficiency of antennas covered by mold compounds is low. Partially opening the QFN at the antenna [4], using film-assisted-molding (FAM) technology, increases radiation efficiency. As a result, the chip is no longer completely encapsulated, expensive fabrication tools are required, and large area cutouts are necessary. That makes this technology inefficient and uneconomic for the use in harsh environmental, low cost measurement systems.

Embedded-wafer-level-ball-grid array (eWLB) technology [5], [6] combines a small chip area and a large antenna aperture using fan-in and fan-out areas in a low-cost approach. On the surface a redistribution layer (RDL) is formed that connects the pads of the chip to solder balls placed in a grid

on the package. However, this is a packaging technology that does not allow visual checks or repairs.

In order to reduce transmission losses, antenna structures are often implemented on chip (AoC) [7]–[9] since lossy interfaces to the package or to the PCB are avoided. In this way, low fabrication tolerances are achieved at the expense of a larger chip area and reduced radiation efficiency on silicon substrate materials [10]. Nonetheless, these concepts require additional lenses to focus the beam [11], which results in a bulky sensor with high restrictions on precise alignment.

This paper presents a novel packaging concept on glass, which allows high integration density on low-cost substrate material and optical transparency. Due to the high structuring accuracy of 9 μm, this technology is attractive for radar applications above 150 GHz. There are basically two options for an efficient radiation from the chip: large antenna aperture or the use of a DWG. This paper presents an ultra compact, mechanically detachable, and low loss transition from a monostatic transceiver MMIC to a DWG. Using a flexible DWG the signal is efficiently distributed due to its low attenuation and mechanical bendability [12], [13]. As a transition from the chip to the DWG, a substrate integrated waveguide (SIW) in glass is applied. Compared to [14], the complexity and number of components were reduced, resulting in an overall insertion loss of 2.85 dB. The integration density in the package is increased by placing the MMIC in a flip-chip process [15]. In order to prevent moisture from entering the air volume via distributed elements and to protect the bare dies from harsh environmental influences, the package concept provides a hermetically sealed encapsulation, thereby enabling a potential application perspective for micro mechanic components like quartz oszillators or micro electro mechanical systems (MEMS).

Initially, the material characterization and the glass processing technology are introduced. In Section III, the system concept and the individual components of the radar system, the MMIC, the DWG fixture in glass, and the polyetheretherketon (PEEK) plug are described and characterized. Additionally, the low loss mm-wave transition to the DWG is presented. Subsequently, Section V discusses the fabrication process and the evaluation of the hermetic seal. The measurement setup of the radar and the presentation of the measurement results are addressed in Section VI, providing a comparison with state-of-the-art solutions. Finally, the paper is concluded in Section VII.

II. GLASS TECHNOLOGY
In order to meet the demand for highly integrated packages for mm-wave radars, glass is used as the substrate material where the MMIC with all its interconnects are integrated on a size of 5.8 mm×4.4 mm. With respect to availability and cost, BF33 glass is a suitable material using LIDE technology [16]. With LIDE, aspect ratios for metalized TGVs larger than 8:1 can be achieved, without degrading the mechanical stability. Compared to fused silica, the thermal expansion coefficient of BF33 is similar to the one of silicon. Furthermore, glass has
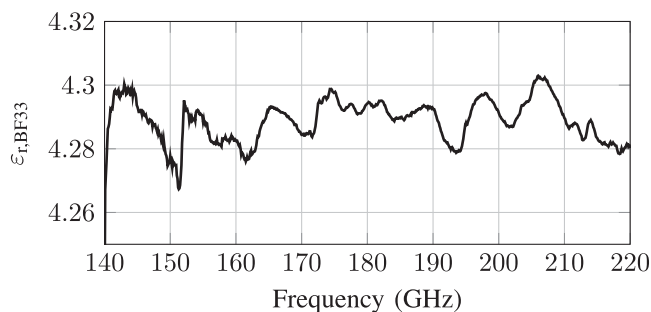

FIGURE 1. Measured relative permittivity $\varepsilon_{\mathrm{r,BF33}}$.

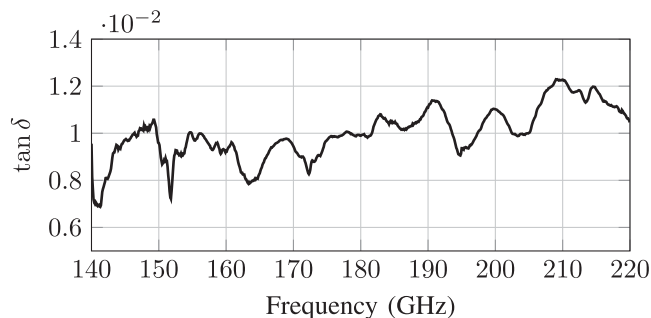**FIGURE 2.** Measured tan δ of the BF33 glass material.

a very low surface roughness of 5 nm, which improves the structural accuracy to 9 μm in the metal sputtering processes. For RF simulations and further optimization design, relevant material properties ($\varepsilon_{\mathrm{r,BF33}}$, tan δ) are needed, which were measured in the frequency band from 140 GHz to 220 GHz using substrate filled waveguides in WR5 cross section [17]. Figs. 1 and 2 show the measured permittivity and dielectric loss, respectively. Due to the optical transparency of glass, visual quality checks of the package can be made without further use of X-ray.

III. PACKAGE REQUIREMENTS AND SYSTEM CONCEPT
The radar MMIC used in this demonstrator operates in the 144 GHz to 163 GHz frequency band and requires 22 pins for input and output connections. The challenge for a packaging concept in this frequency band is to interpose from a 125 μm pitch on chip to the standard 650 μm pitch on PCB. In addition, the bare die has to be encapsulated hermetically to protect it from environmental influences like moisture or gas. This is wholly realized in a package simultaneously offering high integration density, low loss transitions, and high structuring accuracy.

The exploded view of the proposed package is depicted in Fig. 3 presenting the connection to a flexible DWG of HDPE material. The interposer package is based on a stack up of three glass layers housing the flip-chip radar MMIC. Layer ① has a thickness of 500 μm with a cavity of 1700 μm × 2600 μm × 300 μm. Here, vertical TGVs with a diameter of 80 μm form the first vertical interposer connection from standard (650 μm) ball-grid-array (BGA) pitch on PCB. As
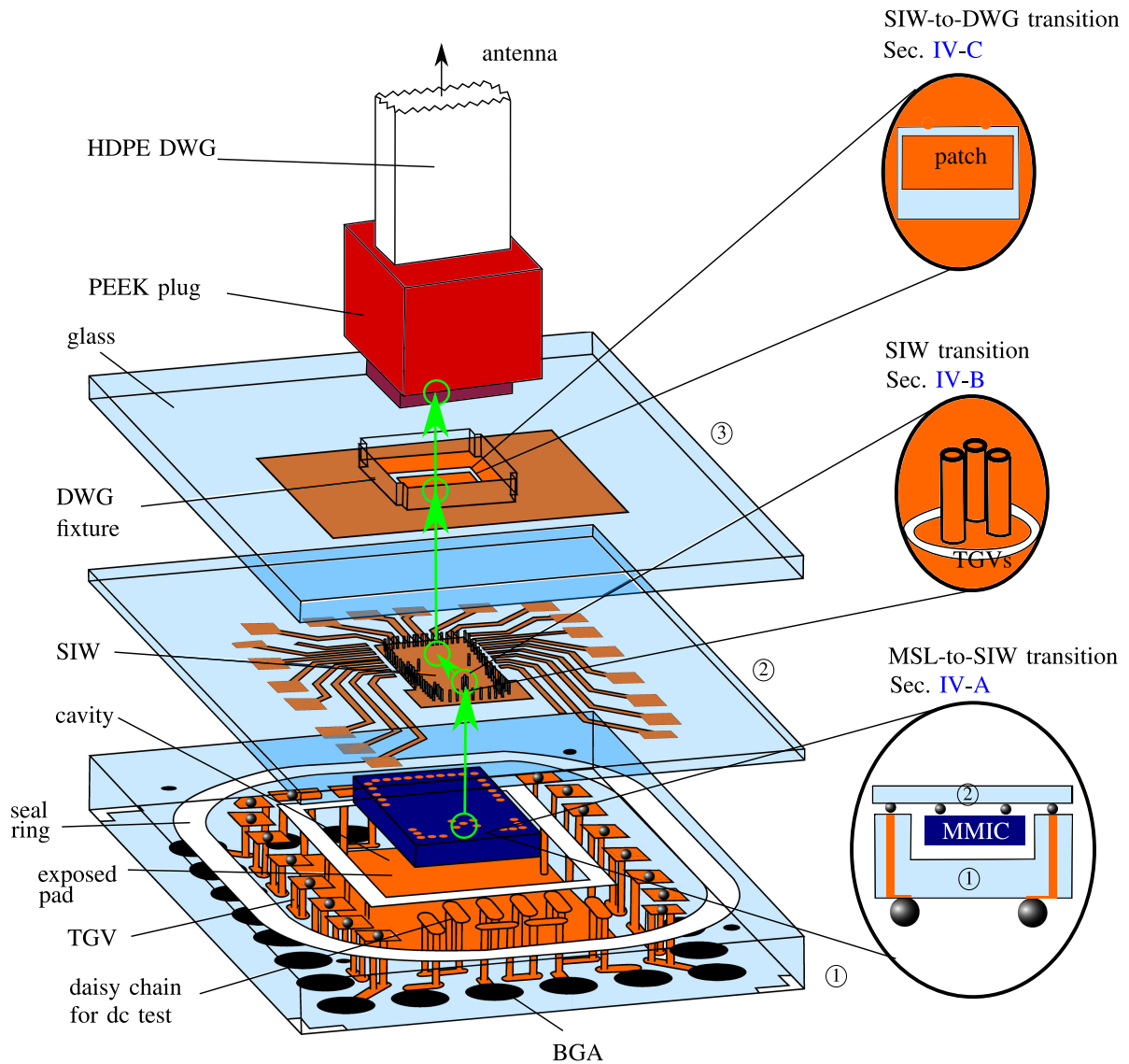
FIGURE 3. Packaging concept for the flip-chip monostatic radar MMIC with transition to the dielectric waveguide. The glass layers illustrated in blue form the substrate material of the package. Glass layer ① represents the low frequency connection to layer ②. The upper glass lid consists of the two single layers ②+③ bonded together with the DWG plugged in guiding the RF signal. A circumferential ring forms the hermetic seal to the lower glass lid. The arrows in green show the RF path from MMIC via SIW into the DWG.

the TGVs with an aspect ratio of up to 5:1 are galvanically plated, the hermetical seal is achieved. To prevent floating potentials in the package, all ground pads are connected with the exposed pad (EP). In the multilayer glass stack up, layer ② with a thickness of 100 μm holds the flip-chip MMIC. Additionally, the transmit and receive signals at 160 GHz are distributed by an SIW structure. Galvanically plated TGVs with a diameter of 20 μm are used to form the side walls of the SIW due to their narrow position. By this approach, a large excitation structure for the DWG is realized on glass for the connection to antennas with a large aperture. The 1.9 mm × 1.1 mm small chip is positioned off-center in the package to establish short signal paths guiding the highest interconnect frequency of 160 GHz. Furthermore, this offers space to integrate an additional daisy chain test structure for

ohmic resistance measurement in the package. The galvanic connection between layers ① and ② is achieved by using 50 μm solder balls. Implementing a circulating ring of lined up solder balls forms a hermetic seal ring between the chip cavity and the outer atmosphere. Copper core balls are partially added to define a constant spacing during the soldering process.

For the further mechanically flexible distribution of the radar signal to a spacially separated antenna, a flexible HDPE DWG is used. The HE$_{11}$ fundamental mode of this waveguide is stimulated by the excitation structure on glass. This is enhanced by implementing a PEEK plug ($\varepsilon_{r,PEEK} = 3.2$) as an interconnection with a higher permittivity compared to HDPE ($\varepsilon_{r,HDPE} = 2.25$) for improved electromagnetic field coupling out of the SIW. Glass layer ③ with a thickness of 200 μm
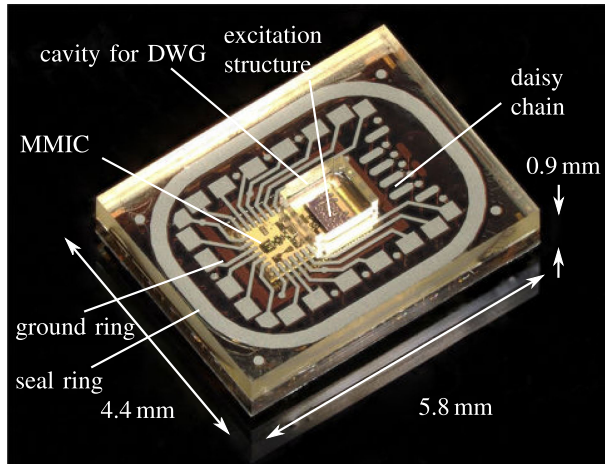
FIGURE 4. Photograph of the proposed hermetically sealed glass package with integrated flip-chip MMIC.
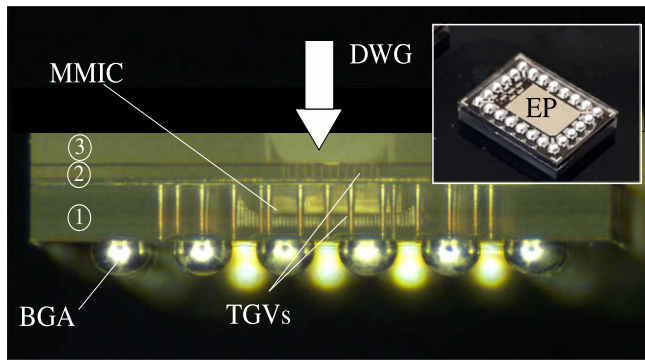

FIGURE 5. Side view photograph of the proposed hermetically sealed glass package showing the vertical TGVs and the flip-chip ASIC in the cavity.

TABLE 1. Dimensions of the Glass Package

y_{PEEK2}	$1050\,\mu m$	i_{HDPE}	$1000\,\mu m$	h_{PEEK1}	$1500\,\mu m$
$d_{pad,\,BGA}$	$50\,\mu m$	x_{HDPE}	$650\,\mu m$	h_{PEEK2}	$500\,\mu m$
$d_{ball,\,BGA}$	$400\,\mu m$	y_{HDPE}	$1295\,\mu m$	x_{PEEK2}	$1100\,\mu m$
$d_{ball,chip}$	$50\,\mu m$	w_p	$650\,\mu m$	l_s	$420\,\mu m$
w_{SIW}	$660\,\mu m$	w_1	$200\,\mu m$	l_p	$250\,\mu m$
$w_{SIW,1}$	$530\,\mu m$	w_2	$320\,\mu m$		
$d_{TGV,(2)}$	$20\,\mu m$	$d_{TGV,(1)}$	$80\,\mu m$		

acts as a clamp fixture for the dielectric PEEK plug in the *x-y*–plane. No further use of bulky mode converters or waveguide steps are necessary. The glass recess is assembled on wafer level and subsequently bonded on the 100 μm thick dielectric layer ②. The realized optical transparent glass package with daisy chain, signal redistribution, and excitation structure are shown in Fig. 4. In Fig. 5 the side view photograph of the realized glass package is depicted, showing the conically shaped TGVs in the package. The solder ball connection to a PCB enables soldering of the package as with the standard ball-grid-array (BGA) assembly. All required dimensions of the glass package and the chip are given in Table 1.
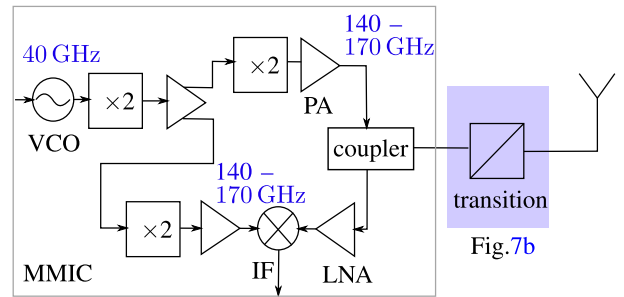
FIGURE 6. Block diagram of the monostatic radar MMIC.
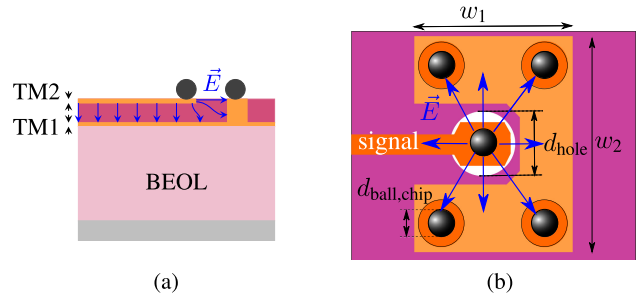
FIGURE 7. RF excitation structure on chip with the electric field distribution illustrated in blue. (a) Cross section of the MMIC. (b)Excitation structure on chip based on MSL transmission line.

The presented radar sensor is based on a monostatic SiGe transceiver MMIC. Fig. 6 shows the chip architecture used in this sensor configuration. The MMIC operates at a center frequency of 156 GHz and provides an RF bandwidth of more than 19 GHz. Thus, a high range resolution of 8 mm is achievable.

IV. TRANSITIONS

In order to emit the high-frequency signal of the radar chip, individual transitions are necessary both on the chip and in the package.

A. MMIC-TO-GLASS LAYER ②

As on-chip antennas enlarge the necessary chip area and raise costs, only a small excitation structure is used on the chip to connect the front-end with a larger physical antenna aperture on glass. A cross section of the MMIC showing the electric field distribution in the back-end-of-line (BEOL) is depicted in Fig. 7(a). Based on the RF port realized in microstrip line technology, a central signal pad and a U-shaped grounding ring are implemented as an excitation structure on the chip. A circular recess in metal layer TM1 with the diameter of $d_{hole} = 80\ \mu$m is directly aligned under the signal pad, which reduces stray field components for improved vertical signal transmission. This results in an RF port structure with a size of 0.32 mm×0.20 mm, which occupies only 3.5% of the chip area. Solder balls with a diameter of 50 μm connect the chip with the metalized bottom layer of dielectric ②. Due to the cylindrical arrangement of the ground solder balls, a quasi-coaxial field distribution is formed, as shown in Fig. 7(b). The
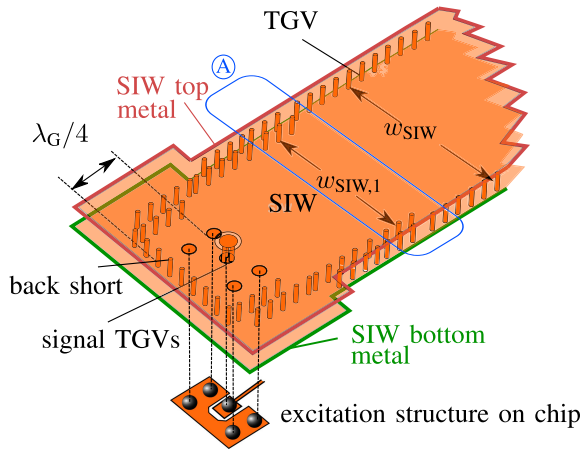
FIGURE 8. Transition from chip to the SIW in glass layer ② consisting of the on-chip excitation, quasi-coaxial signal feeding, and the SIW.
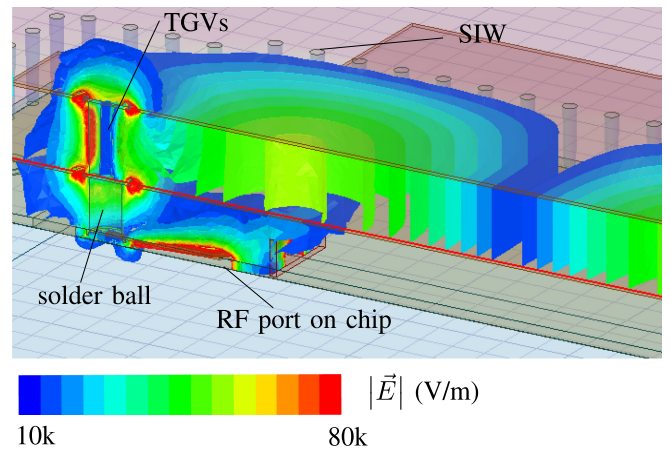

FIGURE 9. $|\vec{E}|$ between MMIC and SIW along the cross section of the SIW.

charcteristic impedance of this line geometry is determined by the pitch between the solder balls. This distance results in turn from the very precise knowledge of the melting behavior of the solder balls. Using this approach, also a direct connection to holographic antenna structures is possible [18].

B. SIW IN GLASS LAYER ②

Fig. 8 illustrates the SIW transition in the glass layer ② consisting of the U-shaped excitation structure complementary on the chip and a stepwise increase of the SIW width for impedance matching. An arrangement of three redundant TGVs with a diameter of $d_{TGV,(2)} = 20$ μm are used to feed the signal vertically through the 100 μm thick layer of glass. Here, the central signal pad on chip connects the stub signal TGVs with a circulating gap ring (10 μm) to the ground metal. Due to the thickness of glass layer ②, this transforms in a short-circuited TGV. For an optimal excitation, this signal feed should be positioned $\lambda_G/4$ apart from the back-wall of the SIW since this is short-circuited by the ground metalization at the top side. λ_G denotes here the guided wavelength. The top and bottom ground metallization of the SIW are connected by a tight chain of vertical TGVs that serve as the electrical sidewall. This is valid for TGV distances smaller than $\lambda_G/10$. As the final SIW width w_{SIW} would result in an abrupt impedance mismatch, $w_{SIW,1}$ is increased stepwise in region Ⓐ. Additionally, inductive posts are added for matching reasons. Fig. 9 illustrates the electromagnetic field distribution along the MMIC-to-SIW transition. Using solder balls, glass layer ② is connected with the MMIC. This forms the vertical quasi-coaxial transition from the chip to the SIW and the further signal propagation in the SIW by the signal TGVs.

C. SIW-TO-DWG TRANSITION

Based on the SIW geometry, a transition into a mechanically flexible dielectric waveguide is presented. The excitation structure for the DWG is depicted in Fig. 10(a) consisting of a patch placed in a recess of the upper metallization of the SIW. This leads to a stimulation of the fundamental mode HE_{11} of
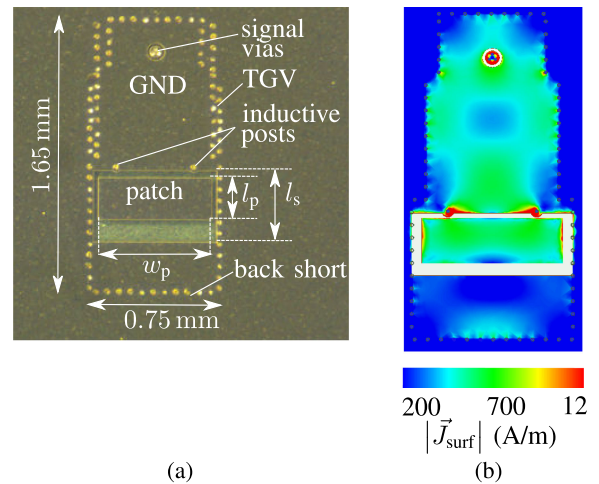

FIGURE 10. (a) SIW structure on the top side of glass layer ② and (b) surface current distribution.

the DWG. Vertical TGVs are arranged closely to the patch acting as inductive posts for matching reasons. The lengths l_p and l_s, see Fig. 10(a), significantly influence the mode properties for the transformation into the waveguide. Due to the integration of the SIW vertically above the MMIC within the pad ring, the width of the patch antenna w_p is limited. Fig. 10(b) illustrates the surface current distribution on the top metal of the SIW. By means of full-wave simulation the patch position and slot dimensions were optimized and are listed in Table 1.

The fixture of the DWG by a simple mechanically detachable clamp connection in glass is a low-cost approach for the waveguide connection. Additionally, this creates numerous degrees of freedom in the optimization of the transmission behavior. No further use of adhesive materials is necessary. The dielectric waveguide in the presented system has a rectangular cross section of 648 μm $\times$ 1295 μm and is made of high density polyethylene (HDPE, $\varepsilon_{r,HDPE} = 2.25$, $\tan\delta = 3.1 \cdot 10^{-4}$ at 160 GHz) assembled in an extrusion process. HDPE combines very low attenuation signal routing (4.5 dB/m) with
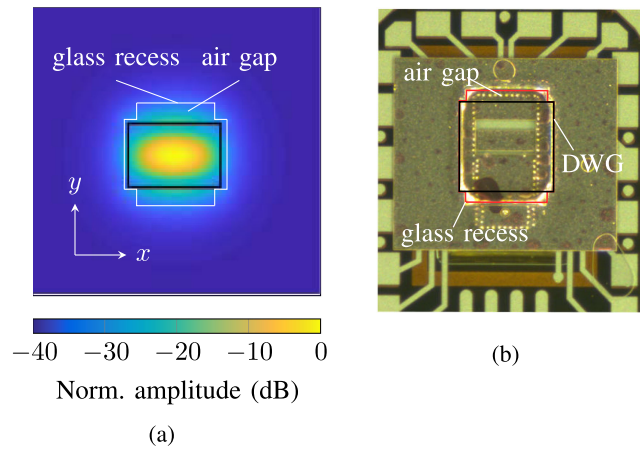
FIGURE 11. (a) Tangential field distribution of fundamental mode of the DWG with (b) corresponding recess in glass.
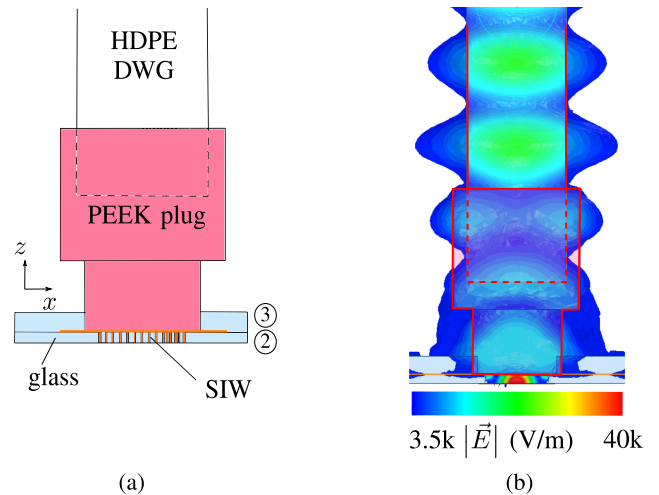

FIGURE 12. (a) Cross section of the SIW to HDPE DWG and (b) electromagnetic field distribution.

FIGURE 13. PEEK plug with corresponding dimensions.

high mechanical flexibility at the same time. For a minimal bending radius of 6 cm a phase delay of 5° is observed. A maximum radiation loss of 0.5 dB occurs at a bending radius of 1.5 cm. For more details on the dielectric waveguide and bending property, see [13].

As the physical contact of a DWG with other dielectric materials shows a strong influence on the attenuation and field distribution [14], the glass contact area is kept as small as possible. Fig. 11(a) shows the field distribution of the fundamental mode of the DWG. The corresponding form of the realized fixture in glass is presented in Fig. 11(b). In order to keep the electromagnetic influence from the glass on the DWG on a minimum, an air gap between glass and DWG is implemented. Therefore, the glass contact areas are located along the short edges x_{PEEK2}. A recess in x-axis disturbs the DWG mode and leads to leakage into the glass substrate. The depth of the recess in layer ③ corresponding to the contact area with glass is set to 200 μm.

Based on the excitation structure on top of the glass layer ②, a dielectric plug made of PEEK material fabricated by a milling process is inserted as an interconnect, as shown in Fig. 12. Due to its higher permittivity of $\varepsilon_{r,PEEK} = 3.2$, the electromagnetic field is more concentrated inside the DWG compared to HDPE material with $\varepsilon_{r,HDPE} = 2.25$. Accordingly, the appropriate mode can be excited whereas parasitic radiation is minimized. In order to maintain the flexibility and low attenuation of HDPE material waveguides, it can simply be inserted into a 1 mm deep groove into the PEEK plug. For an optimal mechanical bending, the height h_{PEEK1} is set as small as possible since PEEK is hardly deformable. The dimensions and the exact shape of the connector are shown in Fig. 13 and Table 1.

D. TRANSITION MEASUREMENT

For characterizing the transition electrically, a back-end-of-line (BEOL) MMIC was fabricated. The BF33 glass of layer ② is metalized with a 10 nm thick titanium layer acting as a seed layer and a subsequent gold metalization with a
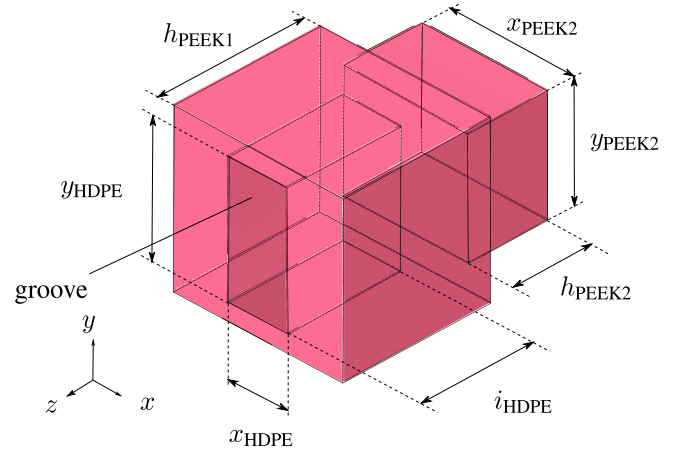
thickness of 4 μm. Afterwards, the metalized glass is soldered on the BEOL chip by a flip-chip process using an alloy of gold and tin (AuSn). As the solder balls have a diameter of 50 μm, the minimum spacing between chip and glass is predefined. For the alignment, high accuracy for the PEEK plug position is required and achieved by the cavity in layer ③, which is bonded with layer ②. A Rohacell stamp clamps the flexible DWG to provide strong fixture in the glass cavity and avoids contact with surrounding metal areas. For the evaluation of the insertion loss and the reflection coefficient, a back-to-back (B2B) measurement setup was used. As presented in Fig. 14, the BEOL MMIC was mounted in an aluminum fixture and contacted with probe tips. Both B2B-transitions were connected by flexible DWGs of different lengths. The difference in length was set to be less than $\lambda_G/2$ in order to meet the unambiguity condition. Subsequently, the transmission and reflection coefficients of the single transition are determined by recalculation from the B2B values. The measured losses of the microstrip line feeding were de-embedded using a through-reflect-line (TRL) calkit on the BEOL chip.
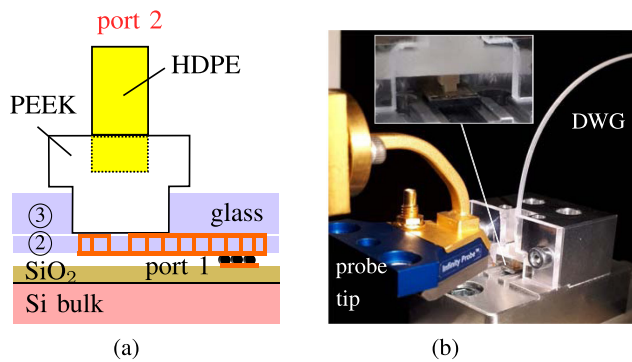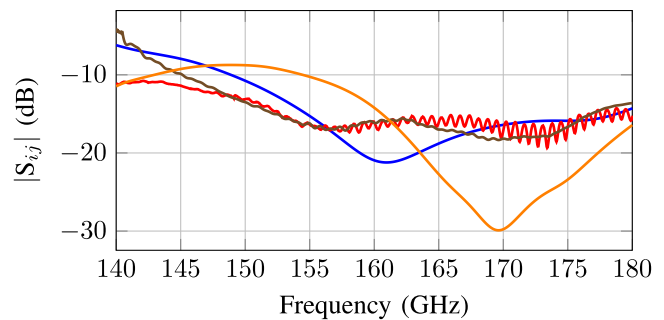
FIGURE 14. Back-to-back setup for the transition measurement using a BEOL MMIC. (a) cross section of the realized transition (b) Back-to-back measurement setup with Rohacell stamp for DWG fixture.
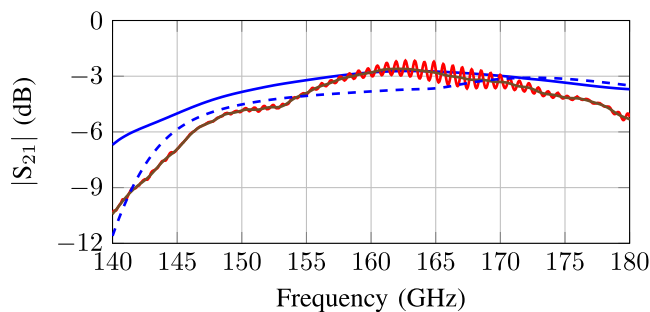

FIGURE 15. Simulated and measured transmission coefficients of the proposed transition using back-to-back measurement (_____ with PEEK plug, _ _ _ without PEEK plug, _____ original measured data, _____ data without probe tips and spurious reflections of the environment).

FIGURE 16. Simulated and measured reflection coefficients of the proposed transition using back-to-back measurement (_____ S_{11} sim, _____ S_{11} original measured data, _____ S_{11} data without probe tips and spurious reflections of the environment, _____ S_{22} sim).
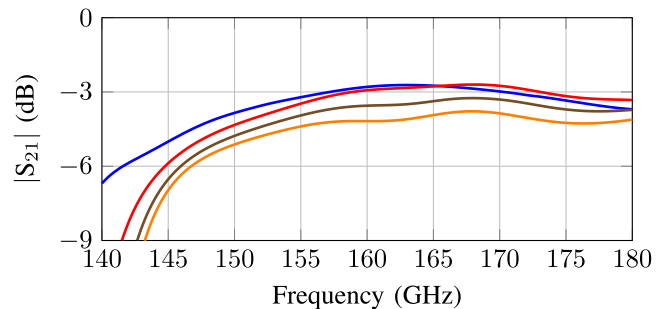
FIGURE 17. Simulated influence of an airgap between PEEK plug and excitation structure on layer ② (_____ 0 μm, _ _ _ 50 μm, _____ 75 μm, _____ 100 μm).

The simulated and measured transmission coefficients from 140 GHz to 180 GHz are denoted in Fig. 15 in which a minimum insertion loss of 2.85 dB is measured at the frequency of 162 GHz. In the frequency range from 156 GHz to 171 GHz, the transmission coefficient drops by 1 dB compared to the maximum. In this setup, the use of an additional Rohacell fixture or mode converters can completely be omitted resulting in a very compact package. As demonstrated in Fig. 15, a strong influence on the insertion loss can be observed, caused by the PEEK connector (solid curve). Compared to the perfect alignment of the DWG, an air gap between glass and PEEK plug shows only a minor influence on the transmission behavior. On the probe side (port 1), the measured reflection coefficient in Fig. 16 is below -15 dB in the frequency range from 152 GHz to 176 GHz. Additionally, the probe tip and spurious reflections from the environment have been removed from the original measurement data by means of time domain gating. The measured values are in close agreement with the simulation results. Fig. 17 shows the low sensitivity of the transmission coefficient to changes of the vertical air gap between the PEEK plug and the patch on the glass layer ②. A reduction of less than 1 dB can be observed for changes of up to 75 μm.

V. PACKAGING ASSEMBLY AND EVALUATION

A major concern regarding RF modules operating at mm-wave frequencies is the repeatable structuring accuracy as conductor circuit dimensions are in the micrometer range. This does not only affect line-gap spacing of conductor circuits but also the position accuracy of TGVs. Using LIDE technology, standard deviations of 0.5 μm for x-y – positions and 0.9 μm for the TGV diameter are achieved. Due to the low change in the surface roughness of R_a= 50 nm during the etching process, high structuring accuracy is still maintained. In this package, each signal line is routed by redundant TGVs, which also reduces the risk of failure. Measurements have been performed to proof the reliability of the TGVs. Temperature cycles in the range of −55 °C and +125 °C were carried out and the results are published in [19]. The resistance measurement via the integrated daisy chain shows the low failure rate of the TGV connection.

A. PROCESS CHAIN

The packaging process, depicted in Fig. 18, starts with the laser modification of BF33 glass wafers and subsequent etching steps, which generate vertical holes for the TGVs and the chip cavity. In a subsequent sputtering process, all metal layers are structured. Since the package should be hermetically sealed, the TGVs are filled and plated galvanically. Then the ASIC is soldered to the glass layer ② in a flip-chip
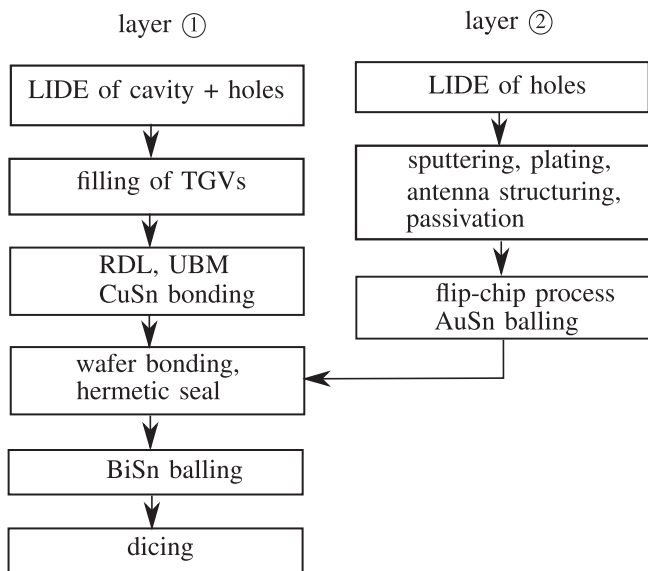
layer ①

| LIDE of cavity + holes |
| filling of TGVs |
| RDL, UBM CuSn bonding |
| wafer bonding, hermetic seal |
| BiSn balling |
| dicing |

layer ②

| LIDE of holes |
| sputtering, plating, antenna structuring, passivation |
| flip-chip process AuSn balling |

FIGURE 18. Work flow of the manufacturing of the packaging concept shown in Fig 4.
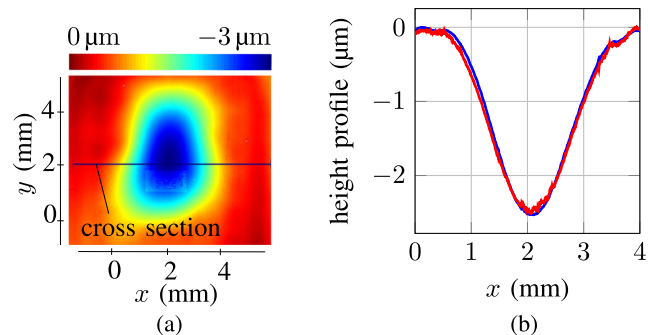

FIGURE 19. Measured topography along the cross section (cut at y=2 mm) in Fig. 19(a); (a) coloured topography (b) Topography measurement along cross section (_____ t_0 = 0 days, _____ t_1 = 100 days).

FIGURE 20. Sensor configuration with dielectric waveguide and dielectric lens from [20].

TABLE 2. System Parameters

Technology	SiGe
Frequency	156 GHz
Mod. bandwidth	19.2 GHz
Sweep time	1024 μs
Number of ramps	128
Chip area	2 mm^2

TABLE 3. Package Internal Link Budget in the Frequency Band From 158 GHz to 162 GHz

Transition	
IL MMIC to SIW (sim.)	0.7 dB
IL SIW to DWG (sim.)	2.1 dB
IL MMIC to DWG (meas.)	2.85 dB
HDPE DWG (meas.)	0.45 dB (4.5 dB/m)
Gain dielectric lens antenna	28 dBi

process. AuSn solder balls are used, as they have the highest reflow temperature within all soldering steps in the package. In parallel, under bump metalization (UBM) and an RDL are structured on glass layer ① in preparation for placing the CuSn solder balls. In a wafer bonding step, glass layer ① is connected to layer ②. The circulating seal ring is obtained by melting the lined up solder balls. Before the individual packages can be diced, BiSn solder balls are placed on the bottom side of the package as connection to the standard PCB material.

B. HERMETIC SEAL INSPECTION

The examination of the hermetic seal of the package is conducted using white light interferometry. A conventional helium leakage test is not applicable here as glass absorbs helium, which distorts the measurement result. Therefore, the height difference of the package surface was measured along a defined cut as illustrated in Fig. 19(a). As the package was fabrica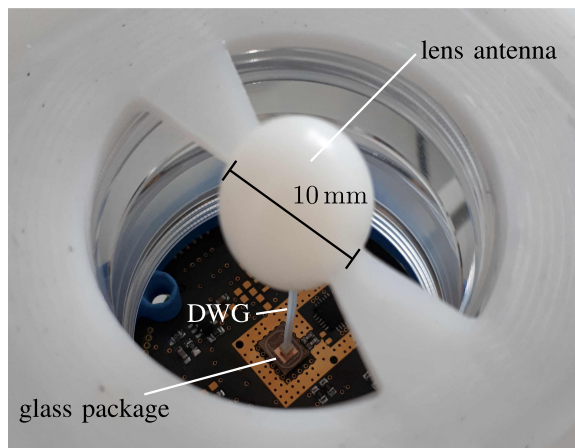ted under vacuum conditions, the inside of the package possesses negative pressure, resulting in a bending of the package surface. The measured height profile along the cross section line in Fig. 19(a) is depicted in Fig. 19(b) and shows that the vertical height difference over the package surface is 2.5 μm. Here, the *x*-axis and *y*-axis display the respective position on the package surface. In order to evaluate the hermetic seal over a longer time period, the measurement was repeated after 100 days using the same package sample. No difference was perceived.
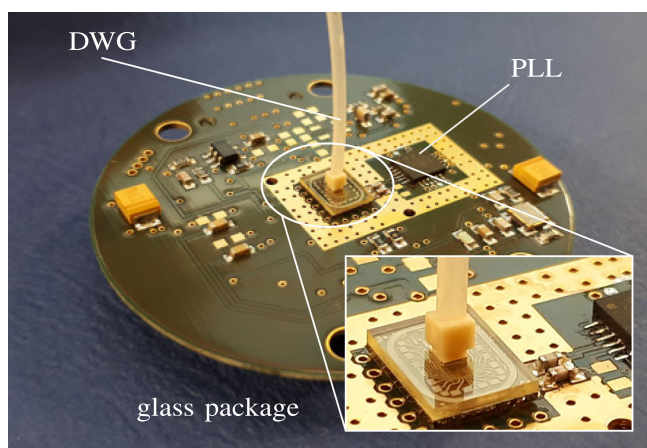
VI. RADAR SENSOR

Measurements were performed with the radar mounted on a linear rail using corner reflectors as targets. Fig. 20 shows the sensor setup with the glass package connected to the DWG and the dielectric lens antenna. This antenna [20] acts as the

TABLE 4. Comparison With the State-of-The-Art

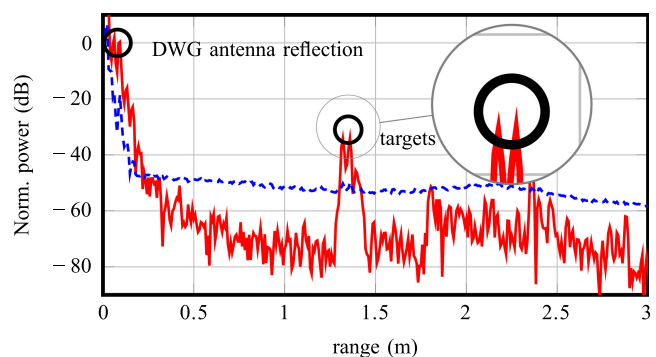| Literature	RF chip excitation	substrate material	substrate parameters @160 GHz (ε_r, $\tan\delta$)	no. of distribution layers	hermetic seal	antenna distance	size (mm)^3	f (GHz)
this work	SIW in glass with patch to DWG	glass	4.29, 0.01	3	yes	2 mm-any length	$5.8 \times 4.4 \times 0.9$	156
[4], [14]	Shortened $\lambda/4$-patch with superstrate, FAM	quartz glass with thermoplast	3.66, 0.004	1	no	3 mm	$5 \times 5 \times 1$	156
[21]	Mushroom electromagnetic bandgap array	LTCC	7, 0.01	1	no	2.4 mm	$7 \times 7 \times 1$	122
[11]	On-chip antenna illuminating silicon lens	LTCC	7, 0.01	2	no	0.005 mm	$8 \times 8 \times 1$	122
[22]	On-chip patch feeding teflon lens	silicon	11.2, 0.02	1	no	10 mm	$5 \times 5 \times 1$	224

FIGURE 21. Radar sensor realized on standard PCB including the baseband circuitry and the radar front end.

FIGURE 22. Measured range spectrum with dielectric lens antenna and corner reflector in 10 mm relative distance and 19.2 GHz RF bandwidth (——— FFT ensemble mean value, _ _ _ FFT standard deviation ramp).

radiating element and can be mounted in arbitrary distances from the package as it is fed by the DWG. The baseband circuitry board, shown in Fig. 21, consists of a phase-locked loop (PLL), baseband filters, and an analog-to-digital converter (ADC). Differential IF output signals of the MMIC are amplified and filtered on the baseband PCB and sampled with 1 MHz using a 16-bit ADC. An on-chip voltage controlled oscillator (VCO) with a bandwidth of 19.2 GHz generates the ramp signal. This setup allows ramp durations from 128 μs to 1024 μs. The system parameters of the setup are listed in Table 2.

A. SENSOR MEASUREMENT

To demonstrate the packaging concept a measurement setup consisting of two corner reflectors with an edge length of 12.7 mm and an appropriate radar cross section (RCS) of

-20 dBsm is used. The radar sensor was mounted on a linear rail at a distance of 1.3 m to the first corner reflector.

A second corner reflector was positioned at a distance of 10 mm relative to the other corner reflector. An up ramp ranging from 144 GHz to 163 GHz with a duration of 1024 μs was used. For the spectral evaluation, a set of 128 measurements was recorded. A Hann window with a side lobe suppression of 31.5 dB is applied to the time signal. For the determination of systematical errors in comparison to thermal noise or phase noise, the Fast Fourier Transform (FFT) of the ensemble mean value and the FFT of the standard deviation ramp are displayed in Fig. 22 . The target peaks at 1.3 m are approximately 20 dB higher than the average noise floor. The reflection caused by the transition from the DWG to the dielectric lens antenna leads to a first target at a distance of 8 cm. A range resolution of approximately 12 mm can be observed. Table 3 breaks down the individual loss contributions obtained by simulation and measurement along the entire RF path in

the package. The total insertion loss of 2.85 dB consists of 0.7 dB for the transition from MMIC to SIW and 2.1 dB for the transition from SIW to HDPE DWG including the PEEK plug. In this setup, the DWG attenuation of 0.45 dB results for the waveguide section of about 10 cm.

B. COMPARISON TO STATE-OF-THE-ART DESIGNS

A comparison with state-of-the-art packaging solutions for operating frequencies above 100 GHz is presented in Table 4. For an holistic comparison not only operating frequency and package size but also material properties, antenna design, and integration density are considered. Compared to other published works [14], an improvement regarding IL at operating frequencies from 140 GHz to 180 GHz was conceived using the glass technology. Due to the cavity for the flip-chip MMIC in glass layer ①, the integration density is enlarged, and the total height of the package is reduced. Additionally, the proposed package concept has three individual distribution layers. This is beneficial for the dimensions of the package, resulting in a total size of only 5.8 mm × 4.4 mm × 0.9 mm. Applying the DWG antenna to the sensor allows an arbitrary distance of the antenna element from the radar MMIC proceeding in a mechanically flexible steering of the antenna field of view. The U-shaped transformer structure on the chip is not only an efficient method to transmit the RF signal from a lossy silicon chip but consumes only 320 μm × 200 μm of chip area.

VII. CONCLUSION

In this paper, a first prototype of a hermetically sealed glass package for radar sensors has been presented, aimed to be used in industrial applications with harsh environmental conditions, thereby providing a cost effective, compact, and robust alternative to conventional packaging concepts. With a tuning range of 19.2 GHz around a center frequency of 156 GHz, high-resolution and high-accuracy measurements are possible. Glass with its low dielectric loss, permittivity, and thermal expansion coefficient is suitable to modern semiconductor chips, as it constitutes a new substrate material which meets the requirements for future mm-wave radar sensors. The package has a total height of only 0.9 mm, including a glass cavity for the flip-chip MMIC. Vertical signal transitions have been realized by TGVs and solder ball connections. The connection to a dielectric waveguide of HDPE materials allows the flexible and low-loss RF signal transmission over a long distance. Based on measurements a minimum insertion loss of 2.85 dB from chip to DWG was evaluated at 162 GHz. The packaging concept is firstly demonstrated by a monostatic radar sensor system, but can easily be extended to MIMO radar configuration in future works. Due to the transparency of glass, easy visual quality control is possible without the use of X-ray. Compared to conventional packaging solutions, the novel package impresses with precise structuring accuracy, hermetic seal, optical transparency, and improved integration density for mm-wave radar sensor technology.

REFERENCES

[1] C. Waldschmidt, J. Hasch, and W. Menzel, "Automotive radar–From first efforts to future systems," *IEEE J. Microwaves*, vol. 1, no. 1, pp. 135–148, Jan. 2021.

[2] M. Serebreni, P. McCluskey, T. Ferris, G. Sharon, N. Blattau, and C. Hillman, "Modeling the influence of mold compound and temperature profile on board level reliability of single die QFN packages," in *Proc. 19th Int. Conf. Thermal, Mech. Multi-Phys. Simul. Experiments Microelectron. Microsyst.*, 2018, pp. 1–8, doi: 10.1109/EuroSimE.2018.8369869

[3] T. Zwick, F. Boes, B. Göttel, A. Bhutani, and M. Pauli, "Pea-sized mmW transceivers: QFN-based packaging concepts for millimeter-wave transceivers," *IEEE Microw. Mag.*, vol. 18, no. 6, pp. 79–89, Sep./Oct. 2017.

[4] M. Hitzler, L. Boehm, W. Mayer, and C. Waldschmidt, "Radiation pattern optimization for QFN packages with on-chip antennas at 160 GHz," *IEEE Trans. Antennas Propag.*, vol. 66, no. 9, pp. 4552–4562, Sep. 2018.

[5] M. Frank *et al.*, "Antenna and package design for 61- and 122-GHz radar sensors in embedded wafer-level ball grid array technology," *IEEE Trans. Microw. Theory Techn.*, vol. 66, no. 12, pp. 5156–5168, Dec. 2018.

[6] A. Hamidipour, A. Fischer, L. Maurer, and A. Stelzer, "A rhombic antenna array solution in eWLB package for millimeter-wave applications," in *Proc. 42nd Eur. Microw. Conf.*, 2012, pp. 205–208.

[7] J. Hasch, U. Wostradowski, S. Gaier, and T. Hansen, "77 GHz radar transceiver with dual integrated antenna elements," in *German Microw. Conf. Dig. Papers*, 2010, pp. 280–283.

[8] J. W. May, R. A. Alhalabi, and G. M. Rebeiz, "A 3 G-bit/s w-band SiGe ASK receiver with a high-efficiency on-chip electromagnetically-coupled antenna," in *Proc. IEEE Radio Freq. Integr. Circuits Symp.*, 2010, pp. 87–90.

[9] M. Hitzler and C. Waldschmidt, "Design and characterization concepts of a broadband chip-integrated antenna," in *Proc. 44th Eur. Microw. Conf.*, 2014, pp. 96–99.

[10] R. A. Alhalabi and G. M. Rebeiz, "Design of high-efficiency millimeter-wave microstrip antennas for silicon RFIC applications," in *Proc. IEEE Int. Symp. Antennas Propag.*, 2011, pp. 2055–2058.

[11] B. Goettel, W. Winkler, A. Bhutani, F. Boes, M. Pauli, and T. Zwick, "Packaging solution for a millimeter-wave system-on-chip radar," *IEEE Trans. Compon. Packag. Manuf. Technol.*, vol. 8, no. 1, pp. 73–81, Jan. 2018.

[12] J. Weinzierl, C. Fluhrer, and H. Brand, "Dielectric waveguides at submillimeter wavelengths," in *Proc. IEEE 6th Int. Conf. THz Electron.*, 1998, pp. 166–169.

[13] M. Geiger, M. Hitzler, S. Saulig, J. Iberle, P. Hügler, and C. Waldschmidt, "A 160-GHz radar with flexible antenna used as a sniffer probe," *IEEE Sensors J.*, vol. 17, no. 16, pp. 5104–5111, Aug. 2017.

[14] M. Geiger, M. Hitzler, W. Mayer, and C. Waldschmidt, "Self-aligning and flexible dielectric waveguide plug for MMICs at G-band," *IEEE Microw. Wireless Compon. Lett.*, vol. 30, no. 3, pp. 261–264, Mar. 2020.

[15] S. Sinha *et al.*, "Flip-chip approach for 500 GHz broadband interconnects," *IEEE Trans. Microw. Theory Techn.*, vol. 65, no. 4, pp. 1215–1225, Apr. 2017.

[16] T. Galler, T. Chaloun, K. Kröhnert, M. Schulz-Ruhtenberg, and C. Waldschmidt, "Hermetically sealed glass package for highly integrated MMICs," in *Proc. 49th Eur. Microw. Conf.*, 2019, pp. 292–295.

[17] T. Zwick, A. Chandrasekhar, C. Baks, U. Pfeiffer, S. Brebels, and B. Gaucher, "Determination of the complex permittivity of packaging materials at millimeter-wave frequencies," *IEEE Trans. Microw. Theory Techn.*, vol. 54, no. 3, pp. 1001–1010, Mar. 2006.

[18] T. Galler, T. Frey, C. Waldschmidt, and T. Chaloun, "High-gain millimeter-wave holographic antenna in package using glass technology," *IEEE Antennas Wireless Propag. Lett.*, vol. 19, no. 12, pp. 2067–2071, Dec. 2020.

[19] K. Kröhnert, G. Friedrich, D. Starukhin, M. Wöhrmann, M. Schiffer, and M. Schneider-Ramelow, "Reliabillity of through glass vias and hermetically sealing for a versatile sensor plattform," in *Proc. IEEE 8th Electron. Syst.-Integr. Technol. Conf.*, 2020, pp. 1–6.

[20] M. Geiger, M. Hitzler, J. Iberle, and C. Waldschmidt, "A dielectric lens antenna fed by a flexible dielectric waveguide at 160 GHz," in *Proc. 11th Eur. Conf. Antennas Propag.*, 2017, pp. 3380–3383.

[21] A. Bhutani, B. Goettel, M. Pauli, and T. Zwick, "122 GHz FMCW radar system-in-package in LTCC technology," in *Proc. 16th Eur. Radar Conf.*, 2019, pp. 373–376.

[22] S. Thomas, C. Bredendiek, and N. Pohl, "A SiGe-based 240-GHz FMCW radar system for high-resolution measurements," *IEEE Trans. Microw. Theory Techn.*, vol. 67, no. 11, pp. 4599–4609, Nov. 2019.

THOMAS GALLER (Graduate Student Member, IEEE) received the M.Sc. degree from Ulm University, Ulm, Germany, in 2018, where he is currently working toward the Ph.D. degree. In 2018, he joined the Institute of Microwave Engineering, Ulm University. His current research interests include antenna-in-package solutions, novel packaging concepts, and microwave monolithic integrated circuit (MMIC) interconnects, all at millimeter-wave frequencies.

TOBIAS CHALOUN (Member, IEEE) received the Dipl.-Ing. and Dr.-Ing. (hons.) degrees in electrical engineering from the University of Ulm, Ulm, Germany, in 2010 and 2016, respectively. From 2010 to 2016, he was a Research Assistant with the Institute of Microwave Engineering, Ulm University, where he conducted his doctoral studies in the field of highly integrated antenna systems for communication applications at millimeter-wave frequencies and has been a Senior Researcher and a Lecturer since 2017. His current research interests include multilayer antennas and circuits, millimeter-wave packaging and inter-connects, phased array antenna systems, and millimeter-wave radar sensors. Dr. Chaloun is a member of the European Microwave Association. He was the recipient of the Best Paper Award at the German Microwave Conference in 2015 and the Best Paper Award of *IET Microwaves, Antennas & Propagation* in 2016. He is currently a reviewer of IEEE TRANSACTIONS ON ANTENNAS AND PROPAGATION and IEEE TRANSACTIONS ON MICROWAVE THEORY AND TECHNIQUES.

WINFRIED MAYER (Senior Member, IEEE) received the Dipl.-Ing. (B.A.) degree in communication technology from the Ravensburg University of Cooperative Education, Germany, in 1994 and the Dr.-Ing. degree from Ulm University, Ulm, Germany, in 2008. From 1994 to 2001, he was with EADS Deutschland Microwave Factory. From 2002 to 2007, he was doing research on imaging radar sensors and digital beam-forming with the Institute of Microwave Engineering, Ulm University. Since 2007, he has been with Endress+Hauser SE+Co. KG, Maulburg, Germany. As a Senior Expert, he has expertise in the fields of industrial radar sensors, mmW-modules, front-ends, and related system aspects. His current research interests interests include innovations for future radar level sensors, including MMICs and mmW-ASICs, low-cost and low-power technologies, system architectures, and new applications. He is working in cooperation with universities, research institutions, and technology partners. He has long-term experience in the transfer of new technologies from research into products. Part-time and since 2015, he has been working on mine detection with UAV-based ground-penetrating synthetic aperture radar in a project of the Urs Endress Foundation.

KEVIN KRÖHNERT studied electrical engineering with the Technical University of Berlin, Berlin, Germany. He received the M.Sc. degree in 2014. In 2008, he started to work as a Student Assistant with Fraunhofer IZM, Berlin, Germany. After his graduation in 2014, he continued to work for Fraunhofer IZM. He is responsible for the PVD, dicing and grinding processes, and the acquisition and realization of various projects regarding microtechnology with the focus on glass interposer and wafer level packaging.

DZMITRY STARUKHIN studied laser physics and spectroscopy with Belarussian State University, Minsk, Belarus. From 2000 to 2004, he was with Physical Institute, TU Chemnitz, Germany. In 2004, he joined the Institute of Physical Chemistry, Uni Heidelberg, Germany, as a Researcher, with focus on time-resolved mid-IR spectroscopy. Since 2013, he has been with Sentronics Metrology GmbH, where he is responsible for sensors and algorithms development.

NORBERT AMBROSIUS studied mechanical engineering with RWTH Aachen University, Aachen, Germany, and received the Dipl.-Ing. degree in 2013 as Dipl.-Ing. He started his career as a Project Manager with Technology Development Department, LPKF Laser & Electronics AG, where he developed the LIDE process. In 2019, he became a Team Leader Process Engineering with LPKF and in that role, he is responsible for the process and technology development of LIDE technology. He is inventor and co-inventor of multiple patents in that field.

MALTE SCHULZ-RUHTENBERG received the Ph.D. degree from the University of Muenster, Muenster, Germany, in 2008. Then, he was with the Fraunhofer Institute for Laser Technology, Aachen, Germany, until 2014. He is currently a physicist specialized in laser technologies. Since 2014, he has been employed with LPKF, first as a Project Leader, later as a Innovation Manager. He is responsible for acquisition and coordination of public funded projects and IP management.

CHRISTIAN WALDSCHMIDT (Senior Member, IEEE) received the Dipl.-Ing. (M.S.E.E.) and Dr.-Ing. (Ph.D.E.E.) degrees from the University of Karlsruhe (TH), Karlsruhe, Germany, in 2001 and 2004, respectively. From 2001 to 2004, he was a Research Assistant with the Institut für Höchstfrequenztechnik and Elektronik (IHE), TH. Since 2004, he has been with Corporate Research and Chassis Systems Business Unit, Robert Bosch GmbH, Leonberg, Germany. He was heading different research and development teams in microwave engineering, RF sensing, and automotive radar. In 2013, he returned to academia. He was appointed as the Director of the Institute of Microwave Engineering, University of Ulm, Ulm, Germany. He authored or coauthored more than 200 scientific publications and more than 20 patents. His research interests include radar and RF sensing, millimeter-wave and submillimeter-wave engineering, antennas and antenna arrays, RF, and array signal processing. Dr. Waldschmidt is currently a Member of the Executive Committee Board of the German MTT/AP Joint Chapter and the German Information Technology Society (ITG). He was the Chair of the IEEE MTT-27 Technical Committee on wireless-enabled automotive and vehicular applications. He was a two-time TPC Chair and the General Chair of the IEEE MTT International Conference on Microwaves for Intelligent Mobility. Since 2018, he has been an Associate Editor for IEEE MTT MICROWAVE WIRELESS COMPONENTS LETTERS (MWCL). He is also a reviewer of multiple IEEE TRANSACTIONS and many IEEE conferences in the field of microwaves. He was a co-recipient of 11 best paper awards.